Available online at www.sciencedirect.com
SCIENCE DIRECT®
Dyes and Pigments 57 (2003) 181–195
DYES and PIGMENTS
www.elsevier.com/locate/dyepig

Crystallographic structures and solid fluorescence behaviors of crystals of a 2-(9-anthryl)phenanthroimidazole-type clathrate host

Lequan Bu[a], Tsuyoshi Sawada[a], Hideto Shosenji[b,*], Katsuhira Yoshida[c], Shuntaro Mataka[d]

[a]*Department of Applied Chemistry and Biochemistry, Faculty of Engineering, Kumamoto University, Kumamoto 860-8555, Japan*
[b]*Institute for Fundamental Research of Organic Chemistry, Kyushu University, Fukuoka 812-8581, Japan*
[c]*Department of Material Science, Faculty of Science, Kochi University, Kochi 780-8520, Japan*
[d]*Institute of Advanced Material Study, Kyushu University, Kasuga-shi, Fukuoka 816-8580, Japan*

Received 13 May 2002; received in revised form 12 October 2002; accepted 14 January 2003

Abstract

The title compound formed crystalline clathrates with ethanol in a 2:1 molar ratio and with water, acetic acid and imidazole in 1:1 molar ratios. The fluorescence behavior of the crystals are greatly dependent on the enclathrated molecules; the intensity increases in order of ethanol < water < acetic acid < imidazole, and the wavelength of the fluorescence maximum is in order of ethanol > water > acetic acid > imidazole. The X-ray crystallographic analyses revealed marked effects of the guest molecules on the intermolecular host-to-host contacts and the intramolecular dihedral angles between the anthryl and phenanthroimidazolyl planes.

Keywords: Solid-state fluorescence; Enclathrated molecule; Inclusion crystal; Guest-dependent fluorescence enhancement; X-ray crystallographic structures; Imidazole-type fluorescent clathrand

1. Introduction

Organic molecules with the ability of forming clathrate compounds have been widely investigated [1,2]. However, only a few clathrate hosts which exhibit sensitive color or fluorescence changes upon inclusion of guest molecules are known [3–5]. Yoshida et al. have recently developed novel heterocyclic quinol-type fluorescent clathrate whose crystals or thin-films exhibit guest-dependent fluorescence enhancement with a blue shift of fluorescence maximum upon formation of clathrates

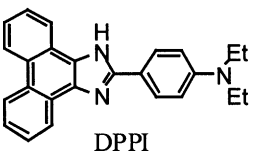

DPPI

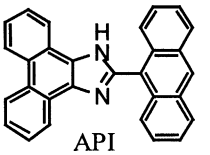

API

* Corresponding author. Tel.: +81-96-342-3670; fax: +81-96-342-3679.
E-mail address: shosenji@chem.kumamoto-u.ac.jp (H. Shosenji).

0143-7208/03/$ - see front matter
doi:10.1016/S0143-7208(03)00020-2

with various organic solvent molecules [6–9]. A drastic fluorescence enhancement with a red shift of fluorescence maximum of 2-[4-(diethylamino)-phenyl-1*H*-phenanthro[9,10-*d*]imidazole (DAPPI) upon contact of its crystals with carboxylic acid vapor have also been reported [10]. These fluorescence enhancements were interpreted in terms of changes in the distances between neighboring host molecules on the basis of the X-ray crystal structures.

Here, we report on a new fluorescent clathrate, 2-(9-anthryl)-1*H*-phenanthro[9,10-*d*]imdazole (API), whose crystals exhibit guest-dependent fluorescence enhancement with a blue shift of emission maximum upon inclusion with guest molecules. The X-ray crystal structures of the clathrate compounds have been determined, and the relationship between the solid-state fluorescence and the changes in crystal structure upon clathrate formation is discussed.

2. Results and discussion

The fluorescent host compound API was prepared according to a slightly modified procedure of the Davidson method [11] known for synthesis of imidazoles. Recrystallizations of API from acetonitrile or ethanol gave needle-shaped enclathrated crystals that contain water or ethanol molecules, while recrystallizations of API from a mixture solvent of acetic acid and acetonitrile or acetonitrile solution of imidazole gave rectangular enclathrated crystals that contain acetic acid or imidazole molecules. In the case of the crystals containing water, the water could come from air atmosphere. The APIs crystals have been milled mechanically, and the solid-state fluorescence of APIs were measured in same cell at same working area (Fig. 1). By the fluorescence measurement we found that a blue shift of the excitation and fluorescence maxima and a guest-dependent

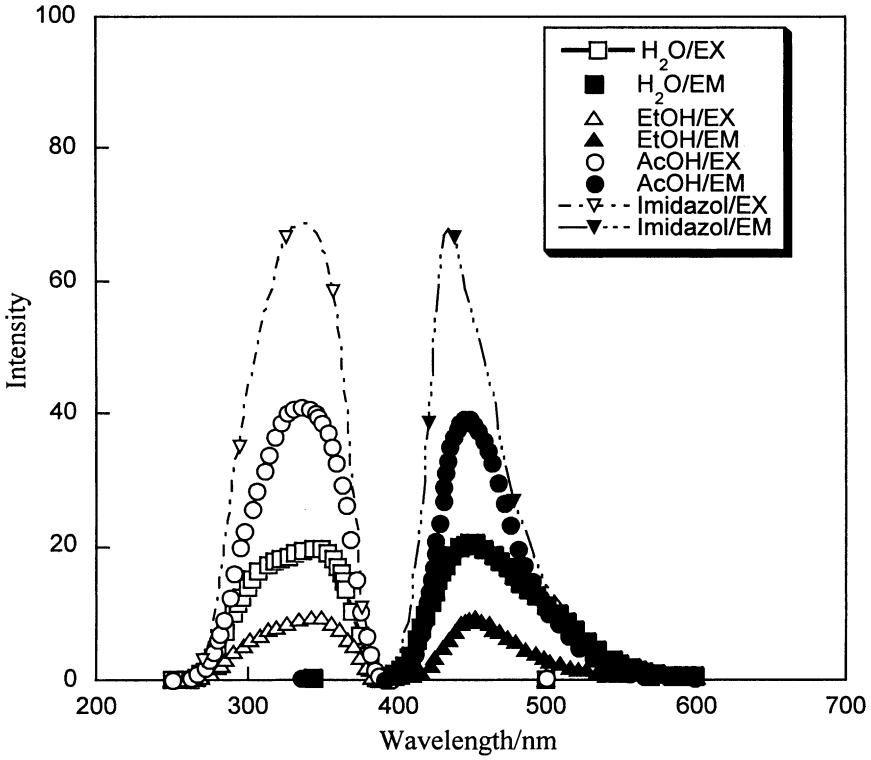

Fig. 1. Excitation and emission spectra of the inclusion crystals of API. EX and EM denote excitation and emission spectra, respectively.

fluorescence enhancement are induced upon inclusion of the guest molecules. Table 1 summarizes the guest-dependent changes in the photophysical properties of the inclusion crystals of API that contain water, ethanol, acetic acid and imidazole molecules. The inclusion crystals were checked by ^{1}H-NMR, which demonstrated that the guest molecules are included into the crystals under specific mole ratios. The host-to-guest stoichiometric ratios were 1:1 in the inclusion crystals of water, acetic acid and imidazole, and 2:1 in that of ethanol. The longest wavelengths of the excitation and fluorescence maxima (λ_{ex} and λ_{em}) were obtained by measuring the solid-state excitation and fluorescence spectra, respectively. The relative fluorescence intensities (RFI) of the inclusion crystals increase in the following order: ethanol < water < acetic acid < imidazole.

To investigate the relationship between the observed photophysical properties and the changes in molecular packing structure upon inclusion of the guest molecules, the crystal structures of the ethanol, water, acetic acid and imidazole inclusion compounds [$(API)_2$EtOH, API·(H_2O), API·AcOH and API·($C_3H_4N_2$), respectively] have been determined by X-ray diffraction analysis and are shown in Figs. 2–6. The dihedral angles (θ) between the anthryl plane and the phenanthroimdazolyl plane estimated from the X-ray crystallography are given in Table 1. The angles increase in the following order: water < ethanol < acetic acid < imidazole. With increasing molecular size of the enclathrated organic molecules the dihedral angle and the fluorescence enhancement become larger except for the ethanol-inclusion crystal, which has a different host–guest molar composition from the other crystals.

In the $(API)_2$·EtOH crystal, host molecules are sequentially linked by the host-to-host NH- - -N, host-to-guest NH- - -O and guest-to-host OH- - -N hydrogen bonds to form a straight molecular chain. Along the chain, there are two types of short host-host contacts. One is the anthryl–anthryl overlapping and the other is the phenanthrene-phenanthrene parts overlapping both with six intermolecular C–C contacts within 3.6 Å. These overlappings suggest aromatic π–π interactions. The long-range host-host interactions based on the intermolecular hydrogen bond and the π–π interaction would cause a strong fluorescence quenching in the ethanol-inclusion crystal.

In the API·(H_2O) crystal, host molecules are alternately linked by the intermolecular NH- - -O hydrogen bond between the imino of phenanthroimidazolyl and H_2O molecules and the OH- - -N hydrogen bonds between H_2O and the nitrogen of the next phenantroimidazolyl to form a linear molecular chain. Along the chain there are three intermolecular C–C contacts between the anthryl and phenanthrene parts with the distances from 3.617 to 3.690 Å; no contact shorter than 3.6 Å is found. Among host molecules in the chains adjacent to each other there are two types of short molecular contacts. One is an anthryl–anthryl type involving two C–C contacts with distances of 3.654 and 3.680 Å; the other is phenanthrene part and anthryl type involving three C–C contacts with distances from 3.571 to 3.600 Å. Indirect linkage by the hydrogen bonding and decrease in

Table 1
Excitation and fluorescence wavelengths, fluorescence intensities, fluorescence lifetimes, host-to-guest mole ratios and the dihedral angles of the inclusion crystals of API

Guest	λ_{ex} (nm)	λ_{em} (nm)	RFI[a]	τ_f (ns)[b]	Host–guest ratio[c]	θ (°)
EtOH	342	452	0.45	0.41	2:1	68.3
H_2O	342	450	1.00	1.03	1:1	66.6
AcOH	336	446	1.95	0.29 (71) 1.29 (29)	1:1	91.2
Imidazole	338	434	3.45	0.56 (58) 1.54 (42)	1:1	101.0

[a] Relative fluorescence intensity at the fluorescence maximum.
[b] The values in parentheses imply the percentages of the fluorescence components.
[c] Determined by means of ^{1}H-NMR integration in DMSO-d_6.

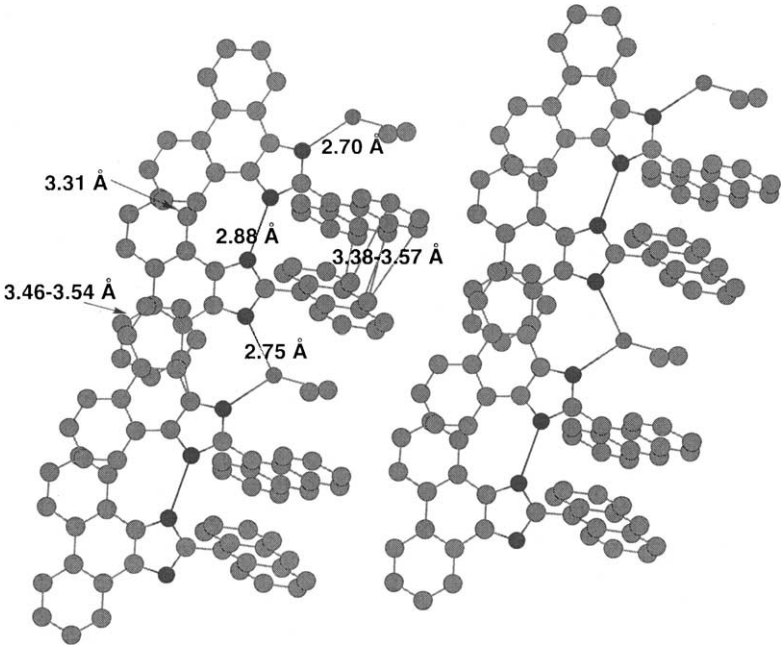

Fig. 2. X-ray crystallographic structure of $(API)_2$·EtOH.

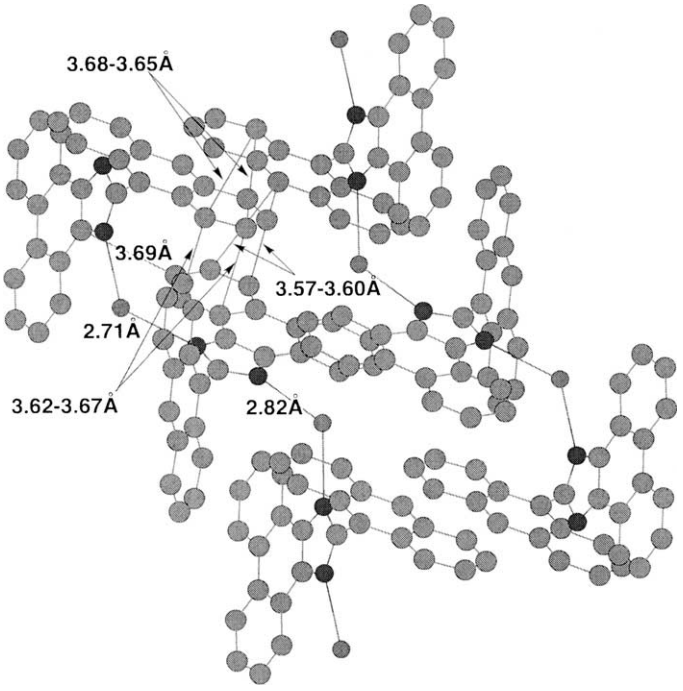

Fig. 3. X-ray crystallographic structure of API·H_2O.

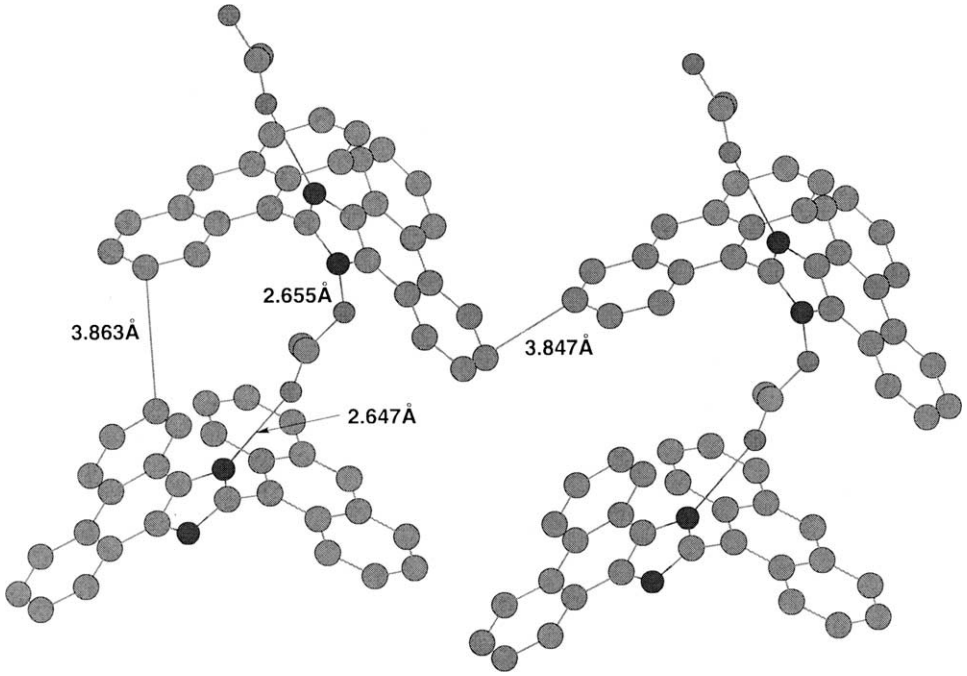

Fig. 4. X-ray crystallographic structure of API·AcOH.

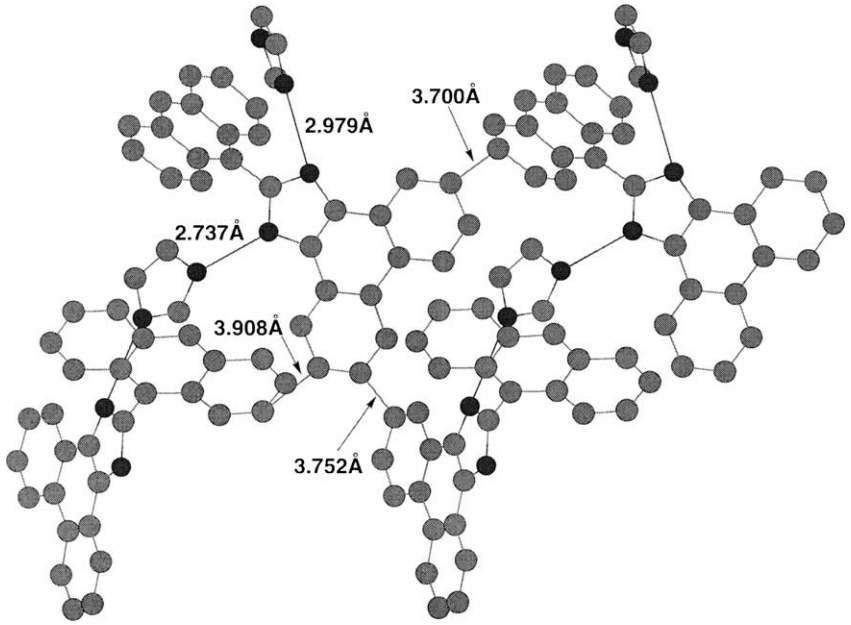

Fig. 5. X-ray crystallographic structure of API($C_3H_4N_2$).

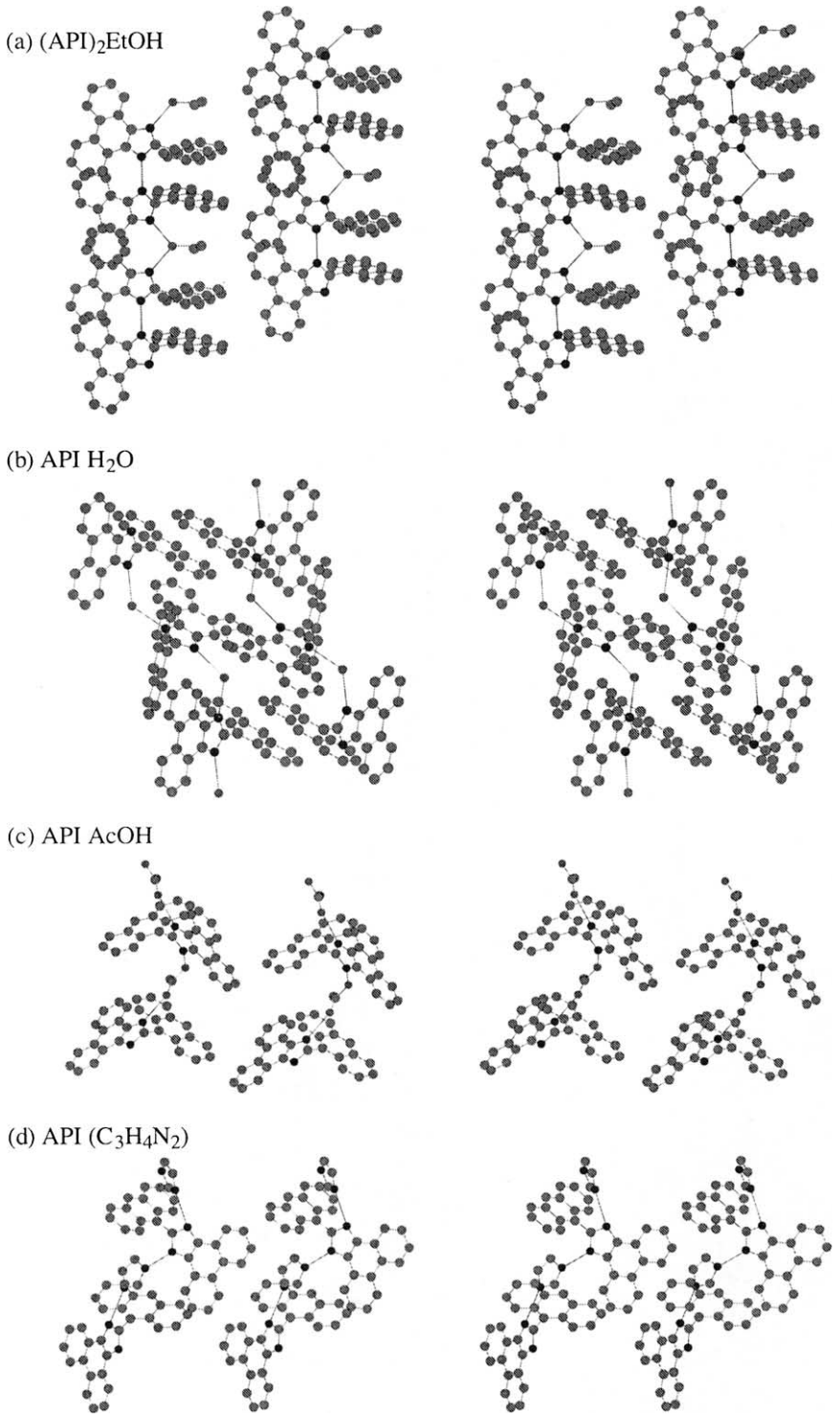

Fig. 6. Stereoviews of crystallographic structure of APIs.

the planar overlapping of the aromatic carbons among the host molecules would reduce the fluorescence quenching, resulting in increase of the fluorescence intensity in comparison to the ethanol inclusion complex.

In the API·AcOH crystal, the host molecules are alternately linked by the NH- - -O and OH- - -N hydrogen bonds among the phenanthroimdazolyls and acetic acid molecule to form an interlaced molecular chain. The host molecules along the chain are linked by the winding pattern with the shortest intermolecular C–C distance of 3.863 Å between anthryl and phenanthrene part. Each chain is separated from adjacent one with the shortest intermolecular C–C distance of 3.847 Å between anthryl and phenanthrene part. As shown in Fig. 4, these aromatic planes are situated in a position almost orthogonal to each other, which is unfavorable for the intermolecular π–π interactions. These steric circumstances around the host molecules may contribute to further increase of the fluorescence intensity.

In the API·($C_3H_4N_2$) crystal, the host molecules are linked by the NH- - -N hydrogen bonds between the imino atom as well as the nitrogen atoms of phenanthroimdazolyl and imidazole molecules to form a molecular chain with a zigzag pattern, in which each anthryl plane is situated almost orthogonal to the phenanthrene plane of the adjacent host. The anthryl plane is also almost orthogonal to the phenanthrene plane of the nearest host in the adjacent chain. The strong fluorescence intensity would be ascribed to the absence of intermolecular planar overlapping between the aromatic nuclei of the host molecules.

DAPPI in the guest free crystals as well as in the inclusion crystals has a conformation with the phenathroimidazolyl and phenyl rings on the same plane [10]. The ultraviolet absorption spectrum of API in ethanol gave extinction coefficient of 1.95×10^4 at the absorption maximum. This is 43% of the value of DAPPI, implying a twisted structure of API derived from a steric hindrance between H of the imino and 1- or 8-H of the anthryl. With a van der Waals radius of 1.2 Å for hydrogen atom [12] the dihedral angle between the phenanthroimidazolyl and anthryl planes is estimated to be 50°. This is close to the values of the water and ethanol inclusion complexes. As shown in Table 1, the acetic acid and imidazol including complexes gave larger dihedral angles. These enclathrated guest molecules with molecular sizes larger than water increase the hollow of the crystal lattice, increasing the dihedral angle of host molecule. API·($C_3H_4N_2$) crystal gave excitation and fluorescence maxima at wavelengths shorter than API·(H_2O) crystal. Blue shifts of excitation and fluorescence maxima are ascribed to the increase of the dihedral angle of host molecule. The crystal of DAPPI including propionic acid showed red shifts of the excitation and fluorescence maxima in comparison to the guest free crystal, which were interpreted as a result of increase of intramolecular charge-transfer character of the host fluorophore caused by hydrogen bonding between the host and guest molecules [10]. On the other hand API·AcOH crystal gave small amount of blue shifts of the excitation and fluorescence maxima in comparison to API·(H_2O), implying that the effect of the twist of molecular structure of the host molecule surpasses the intramolecular charge-transfer character of the host fluorophore by hydrogen bonding.

As shown by Table 1, the host molecules of API·AcOH and API·($C_3H_4N_2$) complexes have conformations, in which the phenanthroimidazole and anthryl planes find themselves almost orthogonal to each other. Thus π-electronic structures of these fluorophors are considered to be independent of each other. This raises a question: which of the aromatic nuclei the fluorescence was emitted from, the phenanthroimidazole or the anthryl part? Calculation of excitation energy was carried out by using the Hyper Chem [13], giving excitation wavelengths of 373.41 and 381.48 nm for the phenanthroimidazole and 388.30 and 390.59 nm for the anthracene. On the assumption that the excitation energy is proportional to the emission energy, the lowest excited state of anthracene is concluded to lie below that of the phenanthroimidazole, in other word, the fluorescence observed was mainly emitted from the anthryl part of the host molecule. Glockner and Wolf have reported the maximum fluorescence wavelength at 399 nm for anthracene in solid state at −195.8 °C [14].

Fluorescence lifetimes (τ_f) of inclusion crystals were measured and the results are summarized in Table 1. The fluorescence of $(API)_2$·EtOH as well as API·(H_2O) was found to be comprised of single components, while two components with shorter and longer lifetimes were observed in that of API·AcOH and API·($C_3H_4N_2$). In the latter case there is a possibility that the fluorescence involves independent emissions from the phenanthroimidazolyl and anthryl parts of the host molecules. Assignments of fluorescence components to the fluorophor require further precise analyses of the fluorescence.

3. Experimental

3.1. General methods

The spectra of solid-state fluorescence were determined with a Shimadzu RF-540 Spectrofluorophotometer. The ultraviolet spectra were measured with a Hitachi U-3210 spectrophotometer. ^{1}H-NMR spectra were observed with a JNM-EX400 spectrometer by using DMSO-d_6 as a solvent. Fluorescence lifetime was measured with Hamamatsu Streak Scope C 4334. Elemental analyses were carried out with a Yanaco CHN Corder MT-6. X-ray diffraction was measured with a Rigaku Raxis-Rapid.

3.2. Preparation of material

3.2.1. Synthesis of API

A mixture of 3.0 g of 9,10-phenanthrenequinone, 3.0 g of 9-anthraldehyde and 17.8 g of ammonium acetate in 50 ml of acetic acid was refluxed for 4.5 h. After cooling the mixture was poured into water, giving yellow precipitates.

3.2.2. $(API)_2$·EtOH

Recrystallization of API from an ethanol gave yellow crystals. Found C, 86.46; H, 5.20; N, 6.74. $C_{60}H_{42}N_4O$ requires C, 86.30; H, 5.07; N, 6.71%. ^{1}H-NMR (DMSO-d_6) $\delta_H = 1.06$ (3H, t, CH_3), 3.45 (2H, q, CH_2), 4.33 (1H, s, OH), 7.51·7.82 (18H, m, ArH), 8.22·8.87 (16H, m, ArH), 13.89 (2H, brs, NH).

3.2.3. API·AcOH

Recrystallization of API from a mixture solvent of acetic acid and acetonitrile (1:5) gave yellow crystals. Found C, 82.03; H, 5.02; N, 6.30. $C_{31}H_{22}N_2O_2$ requires C, 81.92; H, 4.88; N, 6.17%.

3.2.4. API·($C_3H_4N_2$)

Recrystallization of API from acetonitrile solution of imidazole (10%) gave yellow crystals. Found C, 83.49; H, 5.01; N, 12.07. $C_{32}H_{22}N_4$ requires C, 83.09; H, 4.79; N, 12.12%.

3.2.5. API and API·(H_2O)

Recrystallization of API from acetonitrile gave yellow crystals, which contained one molar of water as revealed by X-ray measurement. It was considered that the water came from air atmosphere. Elemental analyses of crystals dried over P_2O_5: found C, 87.80; H, 4.85; N, 7.30. $C_{29}H_{18}N_2$·$0.1H_2O$ requires C, 87.90; H, 4.63; N, 7.07%.

3.3. Crystal data

X-ray crystallographic measurement data of APIs were shown in Table 2.

3.3.1. $(API)_2$·EtOH

$C_{60}H_{42}N_4O$, MW = 834.34, triclinic, space group P-1, $a = 13.8770(19)$, $b = 15.9623(18)$, $c = 10.7584(16)$ Å, $\alpha = 97.971(2)^\circ$, $\beta = 112.855(3)^\circ$, $\gamma = 88.104(3)^\circ$, $V = 2174.2(5)$ Å^3, $Z = 4$ (API:2, EtOH:1), $D_c = 1.275$ g cm^{-3}; Mo K_α radiation (graphite monochromater, $\lambda = 0.71069$ Å) final conventional $R = 12\%$, $R_w = 27.48$ $(F^2)\%$ for observed 3735 reflections [$I > 2\sigma(I)$] and 608 parameters. Atomic coordinates and thermal parameters, and the selected bond length and angles were shown in Tables 3 and 4, respectively.

3.3.2. API·AcOH

$C_{31}H_{22}N_2O_2$, MW = 454.51, monoclinic, space group $P2_1/c$, $a = 12.1637(5)$, $b = 11.9726(4)$, $c = 11.5385(6)$Å, $\beta = 103.523(2)^\circ$, $V = 2341.75(15)$Å^3, $Z = 4$, $D_c = 1.289$ g cm^{-3}; Mo $K\alpha$ radiation (graphite monochromater, $\lambda = 0.71069$Å) final conventional $R = 6.2\%$, $R_w = 18.0$ $(F^2)\%$ for observed 2873 reflections [$I > 2\sigma(I)$] and 374 parameters.

Table 2
X-ray crystal data collected on APIs

Compound	$(API)_2$·EtOH	API·H_2O	API·AcOH	API·($C_3H_4N_2$)
Formula	$C_{60}H_{42}N_4O_1$ (2API and 1EtOH)	$C_{29}H_{20}N_2O$ (1API and 1H_2O)	$C_{31}H_{22}N_2O_2$ (1API and 1AcOH)	$C_{32}H_{22}N_4$ (1API and 1Imidazole)
Mol. wt.	835	412.47	454.51	462.54
Space group	P-1	$P2_1/a$	$P2_1/c$	$P2_1/a$
a (Å)	13.8770(19)	13.2923(11)	12.1637(5)	17.1330(16)
b (Å)	15.9623(18)	14.3204(19)	11.9726(4)	11.8887(8)
c (Å)	10.7584(16)	12.3980(4)	16.5385(6)	23.5992(14)
α (°)	97.971(2)	90	90	90
β (°)	112.855(3)	113.288(2)	103.523(2)	97.120(5)
γ (°)	88.104(3)	90	90	90
V (Å^3)	2174.2(5)	2167.7(3)	2341.75(15)	4769.8(6)
Z	2	4	4	8
D_c (g cm^{-1})	1.275	1.264	1.289	1.288
μ (Mo K_a) (cm^{-1})	0.76	0.77	0.81	0.77
Crystal sizes (mm)	0.30×0.30×0.10	0.50×0.40×0.20	0.50×0.40×0.40	0.40×0.15×0.15
No. unique reflections	9402	4836	5364	9977
No. observed reflections	3735 [$>2\sigma(I)$]	1692[$>2\sigma(I)$]	2873[$>2\sigma(I)$]	3017[$>2\sigma(I)$]
No. variables	608	290	374	650
F(000)	876	864	952	1936
R	0.12	0.141	0.062	0.146
R_w	0.275	0.350	0.180	0.41

Table 3
Atomic coordinates and equivalent isotopic parameters for $(API)_2$·EtOH[a]

Atom	x	y	z	U_{eq}
O1	0.9890(3)	0.2586(4)	0.7461(5)	0.0668(15)
N1	0.8151(4)	0.2045(3)	1.0301(5)	0.0468(13)
N2	0.8652(4)	0.1889(3)	0.8544(5)	0.0432(13)
N3	0.8565(4)	0.3031(3)	1.5035(5)	0.0425(13)
N4	0.8123(4)	0.2960(3)	1.2807(5)	0.0470(13)
C1	0.7294(5)	0.1727(4)	0.9157(6)	0.0461(16)
C2	0.6274(5)	0.1496(4)	0.9041(7)	0.0510(17)
C3	0.5979(6)	0.1489(5)	1.0124(8)	0.063(2)
C4	0.4981(6)	0.1259(6)	0.9919(9)	0.078(3)
C5	0.4259(6)	0.1016(6)	0.8608(9)	0.083(3)
C6	0.4526(5)	0.1006(5)	0.7514(8)	0.068(2)
C7	0.5544(5)	0.1247(4)	0.7669(7)	0.0488(16)
C8	0.5849(5)	0.1227(4)	0.6513(7)	0.0486(16)
C9	0.5129(5)	0.1051(5)	0.5143(7)	0.062(2)
C10	0.5432(6)	0.1034(5)	0.4076(7)	0.068(2)
C11	0.6479(6)	0.1182(5)	0.4297(7)	0.0583(19)
C12	0.7196(5)	0.1362(4)	0.5615(6)	0.0482(16)
C13	0.6898(5)	0.1390(4)	0.6712(6)	0.0455(16)
C14	0.7609(4)	0.1641(4)	0.8094(6)	0.0425(15)
C15	0.8930(4)	0.2132(4)	0.9875(6)	0.0409(14)
C16	0.9996(5)	0.2481(4)	1.0776(6)	0.0433(15)
C17	1.0101(5)	0.3356(5)	1.1207(6)	0.0493(16)
C18	0.9269(6)	0.3924(5)	1.0884(8)	0.063(2)
C19	0.9400(7)	0.4775(6)	1.1288(9)	0.077(2)
C20	1.0428(8)	0.5103(6)	1.2085(9)	0.087(3)

(continued on next page)

Table 3 (*continued*)

Atom	*x*	*y*	*z*	U_{eq}
C21	1.1243(8)	0.4601(6)	1.2421(9)	0.080(2)
C22	1.1144(6)	0.3721(5)	1.1991(7)	0.0564(18)
C23	1.1983(6)	0.3182(5)	1.2278(7)	0.064(2)
C24	1.1883(5)	0.2317(5)	1.1831(7)	0.0579(19)
C25	1.2760(6)	0.1764(6)	1.2098(9)	0.079(3)
C26	1.2634(6)	0.0934(6)	1.1633(9)	0.083(3)
C27	1.1623(6)	0.0584(6)	1.0871(9)	0.082(3)
C28	1.0759(5)	0.1080(5)	1.0605(7)	0.0563(18)
C29	1.0846(5)	0.1946(4)	1.1038(6)	0.0458(16)
C30	0.7547(5)	0.3294(4)	1.4512(6)	0.0418(14)
C31	0.6849(4)	0.3531(4)	1.5172(6)	0.0417(14)
C32	0.7112(5)	0.3519(4)	1.6565(6)	0.0478(16)
C33	0.6402(5)	0.3726(5)	1.7136(8)	0.062(2)
C34	0.5389(6)	0.3935(5)	1.6314(8)	0.067(2)
C35	0.5111(5)	0.3953(5)	1.4965(8)	0.0608(19)
C36	0.5831(5)	0.3747(4)	1.4324(7)	0.0478(16)
C37	0.5548(5)	0.3765(4)	1.2842(7)	0.0500(17)
C38	0.4552(5)	0.4007(5)	1.1969(8)	0.063(2)
C39	0.4319(6)	0.4028(6)	1.0620(9)	0.080(3)
C40	0.5047(6)	0.3810(6)	1.0075(8)	0.085(3)
C41	0.6017(5)	0.3572(5)	1.0886(7)	0.065(2)
C42	0.6281(5)	0.3522(4)	1.2258(6)	0.0504(17)
C43	0.7291(4)	0.3266(4)	1.3159(6)	0.0422(15)
C44	0.8870(4)	0.2835(4)	1.3997(6)	0.0425(15)
C45	0.9929(4)	0.2500(4)	1.4219(6)	0.0409(15)
C46	1.0017(5)	0.1628(5)	1.3884(6)	0.0477(16)
C47	0.9150(6)	0.1038(5)	1.3280(7)	0.0583(19)
C48	0.9289(7)	0.0208(5)	1.3000(8)	0.073(2)
C49	1.0287(8)	−0.0110(6)	1.3265(9)	0.087(3)
C50	1.1136(7)	0.0408(6)	1.3847(8)	0.072(2)
C51	1.1051(6)	0.1300(5)	1.4179(6)	0.0538(18)
C52	1.1919(5)	0.1847(5)	1.4821(7)	0.0576(19)
C53	1.1836(5)	0.2705(5)	1.5180(7)	0.058(2)
C54	1.2717(5)	0.3249(6)	1.5859(8)	0.069(2)
C55	1.2613(6)	0.4084(6)	1.6202(10)	0.080(3)
C56	1.1594(5)	0.4428(5)	1.5889(8)	0.064(2)
C57	1.0740(5)	0.3926(5)	1.5234(7)	0.0540(18)
C58	1.0801(4)	0.3055(4)	1.4872(6)	0.0433(15)
C59A	1.0993(11)	0.2848(10)	0.8243(12)	0.062(4)
C60A	1.1698(14)	0.2143(9)	0.8313(14)	0.078(5)
C59B	1.0914(18)	0.223(2)	0.782(2)	0.033(7)
C60B	1.177(2)	0.291(2)	0.850(3)	0.061(10)

[a] Values in parentheses are estimated standard deviations.

Atomic coordinates and thermal parameters, and the selected bond length and angles were shown in Tables 3 and 4, respectively.

3.3.3. *API·(H_2O)*

$C_{29}H_{20}N_2O$, MW = 412.47, monoclinic, space group P2/a, $a = 13.2923(11)$, $b = 14.3204(19)$. $c = 12.3980(4)$ Å, $\beta = 113.288(2)^\circ$, $V = 2167.7(3)$ Å^3, $Z = 4$, $D_c = 1.264$ g cm^{-3}; Mo K_α radiation (graphite monochromater, $\lambda = 0.7101$ Å) final conventional $R = 14.1\%$, $R_w = 35.0\%$ for observed 1692 reflections [$I > 2\sigma(I)$] and 290 parameters.

Atomic coordinates and thermal parameters, and the selected bond length and angles were shown in Tables 4 and 6, respectively.

Table 4
Selected bond length (Å), bond angles (°) for APIs

	$(API)_2$·EtOH	API·H_2O	API·AcOH	API·($C_3H_4N_2$)
Bond lengths				
N1–C1	1.385(7)	1.373(8)	1.381(2)	1.377(11)
N1–C15	1.346(7)	1.348(8)	1.344(3)	1.388(12)
N2–C14	1.388(7)	1.381(7)	1.388(2)	1.382(11)
N2–C15	1.333(7)	1.321(8)	1.329(3)	1.333(12)
C15–C16	1.492(8)	1.474(8)	1.484(3)	1.462(12)
Bond angles				
C1–N1–C15	106.1(5)	108.0(5)	107.03(17)	106.5(8)
C14–N2–C15	104.0(5)	104.3(5)	104.74(17)	105.0(8)
N1–C15–N2	113.1(5)	112.3(5)	112.16(17)	111.5(7)

Table 5
Atomic coordinates and equivalent isotopic parameters for API·H_2O[a]

Atom	x	y	z	U_{eq}
O1	0.3731(4)	0.1313(3)	0.0686(4)	0.0651(15)
N1	0.5396(5)	0.1937(3)	0.0049(4)	0.0465(14)
N2	0.6786(5)	0.2723(3)	−0.0061(5)	0.0465(14)
C1	0.5555(5)	0.1564(4)	−0.0893(6)	0.0432(15)
C2	0.5027(5)	0.0811(4)	−0.1687(5)	0.0421(15)
C3	0.4142(5)	0.0311(4)	−0.1618(6)	0.0492(17)
C4	0.3682(7)	−0.0422(5)	−0.2396(6)	0.0579(19)
C5	0.4095(7)	−0.0672(5)	−0.3221(6)	0.067(2)
C6	0.4961(6)	−0.0195(5)	−0.3275(6)	0.0548(19)
C7	0.5441(5)	0.0565(4)	−0.2536(5)	0.0442(15)
C8	0.6333(6)	0.1114(4)	−0.2637(5)	0.0443(15)
C9	0.6762(6)	0.0933(5)	−0.3490(6)	0.0593(19)
C10	0.7579(7)	0.1453(6)	−0.3563(7)	0.069(2)
C11	0.8050(7)	0.2187(5)	−0.2786(6)	0.064(2)
C12	0.7659(6)	0.2395(5)	−0.1967(6)	0.0528(18)
C13	0.6816(5)	0.1873(4)	−0.1843(5)	0.0418(15)
C14	0.6410(5)	0.2072(4)	−0.0953(5)	0.0406(15)
C15	0.6139(5)	0.2620(4)	0.0511(5)	0.0434(15)
C16	0.6269(6)	0.3155(4)	0.1573(6)	0.0472(17)
C17	0.5414(6)	0.3777(4)	0.1535(6)	0.0500(17)
C18	0.4485(6)	0.3970(5)	0.0485(8)	0.065(2)
C19	0.3729(7)	0.4599(6)	0.0490(8)	0.078(2)
C20	0.3829(8)	0.5070(6)	0.1516(9)	0.082(3)
C21	0.4705(8)	0.4927(5)	0.2538(9)	0.079(3)
C22	0.5547(7)	0.4280(5)	0.2593(7)	0.059(2)
C23	0.6459(7)	0.4118(5)	0.3636(7)	0.062(2)
C24	0.7317(7)	0.3514(5)	0.3694(6)	0.0549(19)
C25	0.8242(7)	0.3389(5)	0.4744(7)	0.063(2)
C26	0.9080(8)	0.2822(6)	0.4789(7)	0.074(3)
C27	0.8981(7)	0.2333(6)	0.3764(7)	0.070(2)
C28	0.8105(6)	0.2427(5)	0.2730(6)	0.0526(18)
C29	0.7203(6)	0.3028(4)	0.2633(6)	0.0461(16)

[a] Values in parentheses are estimated standard deviations.

Table 6
Atomic coordinates and equivalent isotopic parameters for API·AcOH[a]

Atom	x	y	z	U_{eq}
N1	0.73247(14)	0.32059(13)	0.30544(11)	0.0590(5)
N2	0.71393(14)	0.38324(14)	0.42777(10)	0.0599(5)
C1	0.80516(16)	0.41025(16)	0.32559(13)	0.0544(5)
C2	0.88408(16)	0.45705(17)	0.28256(13)	0.0558(5)
C3	0.89675(19)	0.41752(19)	0.20527(15)	0.0677(6)
C4	0.9751(2)	0.4645(2)	0.16778(17)	0.0789(7)
C5	1.0427(2)	0.5510(2)	0.20774(18)	0.0837(8)
C6	1.03125(19)	0.5917(2)	0.28262(17)	0.0735(7)
C7	0.95068(16)	0.54690(17)	0.32221(14)	0.0581(5)
C8	0.93411(16)	0.59198(16)	0.40137(13)	0.0582(5)
C9	0.99489(19)	0.68462(18)	0.44029(16)	0.0715(7)
C10	0.9774(2)	0.7264(2)	0.51321(18)	0.0778(7)
C11	0.8997(2)	0.6779(2)	0.55188(16)	0.0756(7)
C12	0.83875(18)	0.58701(19)	0.51553(14)	0.0674(6)
C13	0.85468(16)	0.54301(16)	0.44106(13)	0.0565(5)
C14	0.79262(16)	0.44821(16)	0.40050(13)	0.0554(5)
C15	0.67973(17)	0.30839(17)	0.36779(13)	0.0586(5)
C16	0.59124(16)	0.22275(17)	0.36695(12)	0.0545(5)
C17	0.62177(18)	0.11526(17)	0.39694(13)	0.0594(5)
C18	0.7355(2)	0.0825(2)	0.43284(15)	0.0760(7)
C19	0.7614(2)	−0.0223(2)	0.45996(18)	0.0938(9)
C20	0.6761(3)	−0.1028(3)	0.4545(2)	0.1135(11)
C21	0.5668(3)	−0.0755(2)	0.4233(2)	0.1088(11)
C22	0.5350(2)	0.03317(19)	0.39330(16)	0.0729(6)
C23	0.4227(2)	0.0639(2)	0.36036(17)	0.0825(7)
C24	0.39164(19)	0.1692(2)	0.33200(14)	0.0679(6)
C25	0.2772(2)	0.2006(3)	0.30001(18)	0.0881(8)
C26	0.2489(2)	0.3029(3)	0.2706(2)	0.1017(10)
C27	0.3332(2)	0.3845(3)	0.2713(2)	0.0981(9)
C28	0.4441(2)	0.3590(2)	0.30244(16)	0.0792(7)
C29	0.47817(17)	0.25150(17)	0.33390(13)	0.0579(5)
C41	0.6241(14)	0.1643(10)	0.1083(6)	0.195(8)
C42	0.7236(3)	0.1783(4)	0.0757(2)	0.0580(11)
O41	0.6412(5)	0.1971(4)	0.1749(3)	0.1133(16)
042	0.5358(7)	0.1228(7)	0.0501(5)	0.159(3)
C51	0.6115(6)	0.1568(6)	0.1070(4)	0.0422(17)
C52	0.4966(5)	0.1406(5)	0.1457(4)	0.073(2)
O51	0.6845(5)	0.2019(5)	0.1399(4)	0.0746(15)
O52	0.5881(6)	0.0998(6)	0.0367(4)	0.0800(16)

[a] Values in parentheses are estimated standard deviations.

3.3.4. API·($C_3H_4N_2$)

$C_{32}H_{22}N_4$, MW = 462.54, monoclinic, space group $P2_1/a$, $a = 17.1330$, $b = 11.8887$, $c = 23.5992$ Å, $\beta = 97.120(5)^\circ$, $V = 4769.8(6)$ Å ^{3}, $Z = 8$, $D_c = 1.288$ g cm^{-3}; Mo K_α radiation (graphite monochromater, $\lambda = 0.7107$ Å) final conventional $R = 14.6\%$, $R_w = 41\%$ for observed 3017 reflections [$I > 2\sigma(I)$] and 650 parameters.

Atomic coordinates and thermal parameters, and the selected bond length and angles were shown in Tables 4 and 7, respectively.

4. Conclusion

API crystals exhibited guest-dependent fluorescence enhancement with a blue shift of fluores-

Table 7
Atomic coordinates and equivalent isotopic parameters for API·($C_3H_4N_2$)[a]

Atom	x	y	z	U_{eq}
N1	0.7431(5)	−0.1248(6)	0.3974(3)	0.0400(19)
N2	0.6246(5)	−0.0474(7)	0.4033(3)	0.045(2)
N3	0.6332(5)	0.4050(6)	0.1062(3)	0.0381(18)
N4	0.7550(5)	0.3407(6)	0.1173(3)	0.045(2)
N5	0.4797(6)	−0.1356(8)	0.4480(4)	0.067(3)
N6	0.3704(7)	−0.2411(8)	0.4362(4)	0.068(3)
N7	0.3687(6)	0.2872(7)	0.0631(4)	0.058(2)
N8	0.4801(5)	0.3780(6)	0.0607(3)	0.048(2)
C1	0.7341(6)	−0.0381(7)	0.3584(4)	0.038(2)
C2	0.7855(7)	−0.0039(7)	0.3183(3)	0.042(2)
C3	0.8573(7)	−0.0551(9)	0.3138(4)	0.053(3)
C4	0.9032(8)	−0.0204(9)	0.2724(4)	0.065(3)
C5	0.8747(8)	0.0647(10)	0.2351(4)	0.066(3)
C6	0.8065(8)	0.1162(9)	0.2394(4)	0.056(3)
C7	0.7573(6)	0.0860(8)	0.2817(3)	0.044(2)
C8	0.6827(6)	0.1447(7)	0.2877(3)	0.039(2)
C9	0.6597(8)	0.2402(9)	0.2573(4)	0.055(3)
C10	0.5873(8)	0.2918(9)	0.2627(5)	0.065(3)
C11	0.5380(8)	0.2506(9)	0.3006(5)	0.064(3)
C12	0.5637(7)	0.1570(9)	0.3333(4)	0.052(3)
C13	0.6344(7)	0.1038(7)	0.3275(4)	0.044(2)
C14	0.6618(6)	0.0089(8)	0.3630(3)	0.042(2)
C15	0.6751(6)	−0.1271(8)	0.4238(4)	0.043(2)
C16	0.6604(7)	−0.2111(8)	0.4665(4)	0.047(3)
C17	0.6684(6)	−0.1815(8)	0.5243(4)	0.046(2)
C18	0.6940(7)	−0.0752(9)	0.5467(5)	0.059(3)
C19	0.6948(9)	−0.0481(10)	0.6020(5)	0.077(4)
C20	0.6699(9)	−0.1253(12)	0.6411(5)	0.077(4)
C21	0.6475(7)	−0.2284(11)	0.6235(4)	0.062(3)
C22	0.6457(6)	−0.2610(9)	0.5649(4)	0.049(3)
C23	0.6202(7)	−0.3680(9)	0.5449(4)	0.054(3)
C24	0.6154(7)	−0.3994(8)	0.4896(4)	0.050(3)
C25	0.5929(9)	−0.5078(9)	0.4691(6)	0.075(4)
C26	0.5843(9)	−0.5342(10)	0.4134(6)	0.080(4)
C27	0.6018(8)	−0.4510(11)	0.3728(5)	0.072(4)
C28	0.6246(8)	−0.3523(9)	0.3890(4)	0.058(3)
C29	0.6386(6)	−0.3191(8)	0.4481(4)	0.045(2)
C30	0.7503(6)	0.4308(7)	0.1538(3)	0.036(2)
C31	0.8107(6)	0.4832(8)	0.1922(4)	0.041(2)
C32	0.8891(6)	0.4430(8)	0.1978(4)	0.045(2)
C33	0.9499(7)	0.4949(9)	0.2339(4)	0.050(3)
C34	0.9287(7)	0.5883(10)	0.2669(4)	0.058(3)
C35	0.8523(8)	0.6241(9)	0.2616(4)	0.054(3)
C36	0.7914(6)	0.5749(8)	0.2241(3)	0.037(2)
C37	0.7111(7)	0.6200(7)	0.2174(4)	0.046(3)
C38	0.6902(7)	0.7156(8)	0.2460(4)	0.043(2)
C39	0.6156(8)	0.7552(8)	0.2383(4)	0.059(3)
C40	0.5560(7)	0.7032(8)	0.2008(4)	0.050(3)
C41	0.5735(6)	0.6096(7)	0.1712(4)	0.044(2)
C42	0.6502(6)	0.5677(7)	0.1783(3)	0.038(2)
C43	0.6750(6)	0.4720(7)	0.1474(3)	0.037(2)
C44	0.6840(6)	0.3290(7)	0.0908(4)	0.040(2)

(continued on next page)

Table 7 (*continued*)

Atom	*x*	*y*	*z*	U_{eq}
C45	0.6619(6)	0.2459(7)	0.0443(3)	0.042(2)
C46	0.6658(6)	0.2760(7)	−0.0131(4)	0.041(2)
C47	0.6895(7)	0.3824(9)	−0.0281(4)	0.058(3)
C48	0.6926(8)	0.4087(10)	−0.0860(5)	0.071(4)
C49	0.6696(9)	0.3290(11)	−0.1264(5)	0.074(4)
C50	0.6453(8)	0.2262(10)	−0.1142(4)	0.065(3)
C51	0.6415(6)	0.1956(8)	−0.0564(4)	0.044(2)
C52	0.6181(7)	0.0861(8)	−0.0403(4)	0.053(3)
C53	0.6137(7)	0.0566(8)	0.0142(4)	0.054(3)
C54	0.5911(8)	−0.0539(9)	0.0304(5)	0.066(3)
C55	0.5908(9)	−0.0796(10)	0.0846(5)	0.078(4)
C56	0.6092(9)	−0.0019(10)	0.1296(5)	0.076(4)
C57	0.6335(8)	0.1011(9)	0.1175(4)	0.059(3)
C58	0.6371(6)	0.1356(7)	0.0598(4)	0.043(2)
C59	0.4305(7)	−0.1977(12)	0.4127(6)	0.076(4)
C60	0.4489(10)	−0.1366(9)	0.4986(5)	0.081(5)
C61	0.3806(11)	−0.2005(9)	0.4916(5)	0.091(6)
C62	0.4358(8)	0.3188(9)	0.0912(5)	0.064(3)
C63	0.3649(7)	0.3239(9)	0.0085(5)	0.068(4)
C64	0.4353(8)	0.3827(9)	0.0066(5)	0.061(3)

[a] Values in parentheses are estimated standard deviations.

cence maximum upon inclusion of guest molecules. Degree of fluorescence enhancement is in the following order: ethanol < water < acetic acid < imidazole. X-ray crystallographic analysis of ethanol-including crystals revealed long-range host–host interactions based on the intermolecular hydrogen bonding as well as strong π–π interactions, which are considered to cause a strong fluorescence quenching. In water, acetic acid and imidazole including crystals indirect linkings of host molecules through hydrogen bonding involving guest molecules with diminished planar overlapping of aromatic nuclei are considered to reduce the fluorescence quenching. Enclathration of acetic acid and imidazole increased the dihedral angle between anthryl and phenanthroimidazolyl planes of the host molecule, causing blue shift of the fluorescence maximum. Measurements of lifetimes of acetic acid and imidazole including crystals implied independent emissions from the anthryl and phenanthroimidazolyl nuclei of the host molecules. These results indicate that API can be utilized as a chemical solid-sensor for recognition of a variety of guest molecules.

References

[1] Weber E. In: Bishop R, MacNicol DD, Toda F, editors. Comprehensive supramolecular chemistry, vol. 6. Oxford: Elsevier Science; 1996. p. 535.

[2] Bishop R. Designing new lattice inclusion hosts. Chem Soc Rev 1996;25(5):311–22.

[3] Inouye Y, Sakaino Y. Chromotropisms of imidazole derivatives. III. Crystal structure of 4,5-bis(4-methoxyphenyl)-2-(4-nitrophenyl)-1H-imidazole. Bull Chem Soc Jpn 1986; 59(10):3295–6.
Sakaino Y, Takizawa T, Inouye Y, Kakisawa K. Chromotropism of imidazole derivatives. Part 1. 4,5-Bis-(4-methoxphenyl)-2-(4-nitrophenyl)imidazolium acetate dihydrate. J Chem Soc, Perkin Trans 1986;2(10):1623–9.
Sakaino Y, Fujii R, Fujiwara T. Inclusion complexes of a new host, 4,5-bis(4-methoxyphenyl)-2-(4-nitrophenyl)-1H-imidazole, with various guests. J Chem Soc, Perkin Trans I 1990;(10):2852–4.

[4] Kaftory M, Taycher H. Crystal structure and thermochromic behavior of the inclusion compounds of 4,5-diphenyl-2-(4-nitrophenyl)-1H-imidazole and of 4,5-diphenyl-2-(2-hydroxy-5-nitrophenyl)-1H-imidazole. J Chem Soc, Perkin Trans II 1998;(2):407–12.

[5] Brehmer TH, Korkas PP, and Weber E. Sens. Actuators, 1997; B44: 595.

[6] Yoshida K, Yamasaki J, Tagashira Y, Watanabe S. Synthesis of new imidazoanthraquinol fluorophores and

their fluorescence and solid-state inclusion properties. Chem Lett 1996;(1):9–10.
Yoshida K, Tachikawa T, Ymasaki J, Watanabe S, Tokita T. Solid-surface fluorescence characteristics and X-ray crystal structures of inclusion compounds of imidazoanthraquinol-type fluorescent host with ethanol and 1,4-dioxane. Chem Lett 1996;(12):1027–8.

[7] Yoshida K, Miyazaki H, Miura Y, Ooyama Y, Watanabe S. Solid-surface fluorescence enhancement behavior of a benzofuranoquinol-type fluorescent host upon enclathration of alicyclic amines. Chem Lett 1999;(8):837–8.
Yoshida K, Ooyama Y, Tanikawa S, Watanabe S. Fluorescence sensing behavior of thin-films of benzofuranoquinol clathrate host upon exposure to various gaseous amines. Chem Lett 2000;(7):714–5.

[8] Yoshida K, Miyazaki H, Miura Y, Ooyama Y, Watanabe S. Heterocyclic quinol-type fluorophores. Part 1. Synthesis of new benzofurano[3,2-b]naphthoquinol derivatives and their photophysical properties in solution and in the crystalline state. J Chem Soc, Perkin Trans II 2002; (3):700–7.

[9] Yoshida K, Ooyama Y, Tanikawa S, Watanabe S. Heterocyclic quinol-type fluorophores. Part 2. Solid-state fluorescence enhancement behaviour of benzofurano[3,2-b] naphthoquinol-type clathrate hosts upon inclusion of amine molecules. J Chem Soc, Perkin Trans II 2002;(3):708–14.

[10] Yoshida K, Uwada K, Kumaoka H, Bu L, Watanabe S. Fluorescence sensing behavior of crystals of an imidazole-type clathrate host upon contact with gaseous carboxylic acids. Chem Lett 2001;(8):808.

[11] Davidson D, Weiss M, Jelling M. J Org Chem 1937;2:319.

[12] Pauling L. The nature of the chemical bond. Cornell University Press; 1960. 261.

[13] Coleman WF, Arumainayagam CR. J Chem Educ 1998; 75:416.

[14] Glockner E, Wolf HC. Fluorescence spectrum of anthracene crystals. Z Naturforsch A, Astrophys Phys Phis Chem 1969;24:943.